Popular summary of:

Ozone Loss from Quasi-Conservative Coordinate Mapping during the 1999--2000 SOLVE Campaign

During the winter of 1999-2000, the Sage III Ozone Loss and Validation Experiment (SOLVE) field experiment took place in Kiruna, Sweden. The purpose of SOLVE was to examine ozone depletion mechanisms in the Arctic stratosphere (from about 10 to 50 km altitude) during the winter and early spring, when a band of strong winds (the "polar vortex") circle the pole. Measurements of stratospheric ozone were made by several different kinds of instruments in different meteorological situations. We analyzed these data using the "quasi-conservative coordinate mapping" technique, in which the measurements are analyzed in terms of meteorological properties ("potential temperature" and "potential vorticity") which tend not to change very much over a few days. This technique reduces or removes the changes that are associated with the polar vortex moving around. Over longer time periods, potential temperature and potential vorticity change as air cools and descends within the polar vortex. We account for these changes by calculating the trajectories of air parcels, and this enables us to extend the analysis over a ten-week period from January 10 to March 17, 2000. Using data from the NASA ER-2 aircraft, from the DIAL and AROTEL laser sounders on the NASA DC-8 aircraft, and balloon-borne ozonesondes, our analysis reveals changes in ozone which, because we have removed the effects of polar vortex motion and the descending air, indicate chemical destruction of ozone in early 2000. We find a peak decline rate of approximately 0.03 ppmv/day near 470 Kelvin of potential temperature (near 20 km) in mid-January which sinks in altitude to around 440 Kelvin (near 18 km) in mid-March.

Ozone Loss from Quasi-Conservative Coordinate Mapping during the 1999–2000 SOLVE Campaign

L. R. Lait

Science Systems and Applications, Inc., Lanham, MD

M. R. Schoeberl, P. A. Newman, T. McGee, J. Burris

NASA Goddard Space Flight Center, Greenbelt, MD

E. V. Browell

NASA Langley Research Center, Hampton, Va

E. Richard

NOAA Aeronomy Laboratory and U. Colorado, Boulder, CO

G. O. Braathen, B. R. Bojkov

Norwegian Institute for Air Research, Norway

F. Goutail

Centre National de la Recherche Scientifique, France

P. von der Gathen

Alfred Wegener Institute for Polar and Marine Research, Potsdam, Germany

E. Kyrö

Finnish Meteorological Institute, Sodankyla, Finland

G. Vaughan

University of Wales, Aberystwyth, UK

H. Kelder

Royal Netherlands Meteorological Institute (KNMI), De Bilt, The Netherlands

S. Kirkwood

Swedish Institute of Space Physics, Sweden

P. Woods

National Physical Laboratory, UK

V. Dorokhov, I. Zaitcev

Central Aerological Observatory, Moscow, Russia

Z. Litynska

Institute of Meteorology and Water Management, Legionowo, Poland

A. Benesova, P. Skrivankova

CHMI (Czech Hydrometeorological Institute), Prague, Czech Republic

H. De Backer

KMI/IRM (Royal Meteorological Institute of Belgium)

J. Davies

Atmospheric Environment Service/Canada, Ontario, Canada

T. Jorgensen, I. S. Mikkelsen

Danish Meteorological Institute, Copenhagen, Denmark

Short title: OZONE LOSS FROM RECONSTRUCTION

Abstract.

Ozone observations from the AROTEL and DIAL lidars on board the NASA DC-8 aircraft, the NOAA in situ instrument on board the NASA ER-2 aircraft, and THESEO 2000 ozonesondes are analyzed using a quasi-conservative coordinate mapping technique. Measurements from the late-winter/early-spring SOLVE period (January through March 2000) are incorporated into a time-varying composite field in a potential vorticity-potential temperature coordinate space; ozone loss rates are calculated with and without diabatic effects. The loss rate from mid-January to mid-March near the 450 K isentropic surface in the polar vortex is found to be approximately 0.03 ppmv/day.

1. Introduction

Since the discovery of the Antarctic ozone hole by *Farman et al.* [1985], stratospheric researchers have monitored the ozone layer, watching for signs of similar chemical processes over the Arctic regions. To detect ozone loss, researchers have collected and analyzed measurements from satellite instruments such as the Total Ozone Mapping Spectrometer (TOMS) and Microwave Limb Sounder (MLS). (*Newman et al.* [1997] and *Manney et al.* [1997] are examples.) Just as important, however, have been data from field experiments such as the Airborne Arctic Stratospheric Expeditions (AASE I and II), as outlined in *Turco et al.* [1991] and *Rodriguez* [1993]. Measurements from such experiments typically involve a large number of species from relevant families of atmospheric constituents, and these data—frequently of high spatial and temporal resolution—enable a fairly detailed understanding of the chemical processes associated with stratospheric ozone loss. (See, for example, *Salawitch et al.* [1993].)

During the winter of 1999-2000, the Sage III Ozone Loss and Validation Experiment (SOLVE) was carried out simultaneously with the Third European Stratospheric Experiment on Ozone (THESEO) campaign. Meteorological and trace gas constituent data were collected by many different in situ and remote sensing instruments. These included measurements of stratospheric ozone by airborne lidars, an airborne UV-absorption photometer, and ozonesondes.

Given SOLVE's and THESEO's variety of ozone measurements taken by different instruments at different times and scattered locations, it is desirable to put these data into

a consistent wide-scale meteorological framework. As outlined in *Schoeberl and Lait* [1991], constituent mapping using quasi-conserved coordinates can be a useful technique for this purpose. A composite field of trace gas constituent measurements is constructed in a vortex-relative coordinate system using potential vorticity (PV) and potential temperature (θ) as abscissa and ordinate, respectively. Then, given gridded meteorological fields of PV and θ, one can map the composite into real space, creating a three-dimensional field of the reconstructed constituent. *Schoeberl et al.* [1989] and *Lait et al.* [1991] demonstrate examples of this "PV-θ" technique. Related techniques are employed in *Manney et al.* [1994] and *Kyrö et al.* [2000].

In this paper, we refine the PV-θ technique and use it to investigate ozone depletion observed during the late winter/early spring of 2000. Section 2 describes the data used in this analysis, and Section 3 describes the enhanced technique. Results are presented in Section 4, and the conclusions follow.

2. Data

2.1. Meteorological Data

PV-θ analysis requires that each measurement be associated with a value of PV and θ, and PV at least must be obtained from gridded meteorological analyses. Three sources of such analyses were used for this work.

The NASA Goddard Space Flight Center's Data Assimilation Office (DAO) product for the SOLVE period is obtained from their GEOS-3 assimilation system for EOS-Terra support.

GEOS-3 is the successor to the GEOS-1 system documented in *Pfaendtner et al.* [1995]. These data grids extend from 1000 hPa to 0.2 hPa, have a horizontal resolution of 1° longitude by 1° latitude, and are produced four times daily.

The United Kingdom Meteorological Office (UKMO) product generated for the Upper Atmosphere Research Satellite (UARS) project is another assimilation effort, described in *Swinbank and O'Neil* [1994]. The version used here extend from 1000 hPa to 0.4 hPa, have a horizontal resolution of 3.75° longitude by 2.5° latitude, and are produced once per day.

The third source of meteorological data is from the long-term assimilation performed by the National Centers for Environmental Prediction (NCEP) and the National Center for Atmospheric Research (NCAR) The NCEP/
NCAR reanalysis system's procedures are applied consistently to over 40 years of raw data, resulting in a dataset which is useful for long-term studies. (For further information, see *Kalney et al.* [1996]). These data extend from 1000 hPa to 10 hPa, have a horizontal resolution of 2.5° longitude by 2.5° latitude, and are produced four times daily.

To account for diabatic effects, heating rates were calculated from the UKMO analyses using the model described in *Rosenfield et al.* [1994].

2.2. Ozone Data

SOLVE consisted of three deployments: December 2–14, 1999; January 10–February 3, 2000; and February 26–March 16, 2000. During these periods, the NASA DC-8 and ER-2 aircraft flew numerous sorties out of Kiruna, Sweden.

On board the ER-2, a dual beam UV-absorption photometer measured ozone volume

mixing ratios at flight altitudes (above 18 km). *Proffitt and McLaughlin* [1983] describe the instrument. These data are well-calibrated and of good accuracy (around 3%). And at one measurement per second on an aircraft moving at approximately 200 m/s, they have high spatial and temporal resolution. However, their coverage is limited to the actual position of the aircraft.

In contrast, two lidar instruments on board the DC-8 measured profiles of ozone above the aircraft well into the stratosphere. The UV Differential Absorption Lidar (DIAL) measurements have a vertical resolution of approximately 750 m and are taken at least five minutes apart (giving a horizontal resolution of up to 70 km). DIAL profiles reach to 25 or 30 km. DIAL measures ozone number densities, and the DAO analyzed temperatures are used to convert to volume mixing ratios. See *Browell et al.* [1998] for further description of the instrument.

The Airborne Raman Ozone and Temperature Lidar (AROTEL) uses Rayleigh and Raman scattering to obtain profiles with a vertical resolution of 0.5 to 1.5 km and which are taken at least 2 minutes apart (giving a horizontal resolution of up to 24 km). AROTEL profiles reach up to 35 to 40 km. Like DIAL, AROTEL measures ozone number densities, but AROTEL uses its own temperature measurements to convert to volume mixing ratios. *McGee et al.* [in this issue] describe this instrument in more detail.

These three aircraft-based instruments provide stratospheric ozone measurements of high resolution along their flight tracks which cut cross large areas of the Arctic between Greenland and Novaya Zemlya. They are limited to flight days within the three SOLVE deployment periods, however.

Ozonesondes launched by the THESEO campaign, the Canadian Atmospheric Environment Service, the World Meteorological Organization network, and Russia measured profiles at a number of sites in the Arctic. Using an electrochemical concentration cell, these instruments take measurements with a vertical resolution of 8 to 50 m and typically reach up to around 30 km. Although the launch sites are geographically sparse, these profiles exist for nearly every day of the period examined here.

3. Analysis

PV was obtained from the meteorological analysis closest in time to each measurement by interpolating the gridded field bilinearly in the horizontal and using cublic spline interpolation in log-pressure for the vertical. The lidar instruments' profiles are a function of geometric height above the aircraft; the analyzed geopotential heights on pressure surfaces were converted to geometric heights and used to obtain the pressure of each measurement along the flight track . Modified PV (*Lait* [1994]) was used to avoid the strong vertical scaling exhibited by regular Ertel's PV. For consistency, the θ values were similarly interpolated from the meteorological analyses, even for instruments which measured temperature.

A time-varying ozone composite was constructed on a grid in PV-θ space. The edges of the grid were chosen to be well-removed from the values typical of the area of interest (the Arctic lower stratosphere): 0 to 50 PV Units (One PVU being one $10^6 \mathrm{K\ m^2/kg-s}$) and 200 to 1000 K in θ. The grid coordinates were nondimensionalized to a rectangle with an aspect ratio on the order of unity.

A reasonably long-lived trace gas is expected to be well-mixed along contours of PV on a

surface of constant θ (Leovy et al. [1985]), and in the absence of diabatic affects and chemical changes a simple composite made by averaging mixing ratios near a gridpoint should yield an accurate picture of a time-invariant trace gas distribution in PV-θ space.

But over the course of the ten weeks examined here one cannot neglect diabatic effects or chemical ozone loss. Both effects appear as a change in ozone mixing ratio at a given point in PV-θ space. One must take into account this time-varying nature of the field when creating the PV-θ composite.

Over periods of a few weeks (shorter than seasonal time scales), the ozone mixing ratio χ at fixed PV and θ values can be approximated as a linear change in time t:

$$\chi(\mathrm{PV}, \theta) = a(\mathrm{PV}, \theta) + b(\mathrm{PV}, \theta)t \tag{1}$$

To make the ozone PV-θ composite, constants $a(\mathrm{PV}, \theta)$ and $b(\mathrm{PV}, \theta)$ were computed by constructing a time series at each gridpoint of all the nearby ozone measurements. A linear least-squares fit in time was applied to the measurements, which were weighted by

$$w_i = (1 + 1/\sqrt{\sigma_i}) \exp(-d_i^2) \tag{2}$$

where σ_i is the estimated or quoted uncertainty in the ith measurement and d_i is a scaled nondimensional distance from the ith measurement to the gridpoint in PV-θ coordinates. A typical time series and fit for the ozonesonde data is shown in Figure 1.

Figure 1

The results of the time fits are two PV-θ grids a and b, containing slopes and intercepts, respectively. An ozone field in PV-θ space can be reconstructed from these for any day. Given PV and θ fields at points in real space, this reconstructed ozone grid can be mapped onto those points to obtain nominal values of ozone there. Figure 2, for example, shows ozonesonde data

Figure 2

which has been mapped onto vertical profiles above the NASA DC-8 for comparison with the AROTEL data. The figure shows the comparison for the flight of March 9, when the DC-8 flew back and forth across the vortex edge. The remapped sonde data generally compare well with the AROTEL measurements. Two properties of the reconstructed field stand out. First, its spatial resolution is much less than that of the original data. This is not surprising, considering the averaging process and the limited resolution of the meteorological analyses. Nevertheless, the reconstructed field does show the edge structure clearly. Second, the reconstructed ozonesonde data cover a much larger part of the flight than the actual AROTEL measurements. This is true despite the fact that the raw sonde profiles are much more sparsely distributed over the Arctic region than the AROTEL profiles. The reconstruction process assumes that the average of ozone values measured under certain meteorological conditions will be typical of all ozone values in identical conditions, and maps them accordingly.

In a similar way, one can use gridded three-dimensional fields of PV and θ to map the ozone composite onto the fields' grid points to obtain an ozone field covering a large area. After using climatological values to fill in regions above and below the reconstructed profiles, such a field can be integrated vertically, yielding a total ozone field that can be compared with TOMS measurements. A comparison for a typical day is shown in Figure 3. PV-θ reconstruction reproduces the morphology of the total ozone field fairly well, and the values themselves are reasonable. The lower total ozone values from the reconstruction are higher than the TOMS measured values. Inspection of ozonesonde and reconstructed ozone profiles indicates that these differences are chiefly caused by uncertainties in the reconstructed values in the lowermost stratosphere/upper troposphere, where small variations in ozone mixing

Figure 3

ration can result in large variations in total ozone.

Reconstructed fields can be used to determine ozone change rates by differencing the fields at the beginning and end of a time period, or by mapping the slopes from the least-squares fits into real space. However, the change caused by diabatic descent of air in the polar vortex and the change caused by chemical destruction of ozone will be indistinguishable. A way is needed to account for the diabatic descent to enable the rate of chemical destruction to be determined. Two methods for accounting for diabatic effects were used in this analysis.

To determine how much descent took place within the vortex over this period, air parcel trajectories were traced using an isentropic trajectory model with diabatic corrections (See *Schoeberl et al.* [1998], but here the net diabatic heating rate is not balanced). Parcels were initialized at approximately equally-spaced gridpoints on θ surfaces spaced 10 K apart from 400 K to 600 K, and the trajectories were run both forward and backward between January 10 and March 18 using the UKMO meteorological data and heating rates from the Rosenfield model.

To obtain descent rates within the vortex core, only those parcel trajectories which started out and ended up in the core of the vortex were retained. The vortex core was found by determining the PV value that marks the highest 10% all PV values on the (equidistant) gridpoints which lie poleward of 50° N on each theta surface. These PV values were used to delimit the core of the vortex on the beginning and ending dates; this practice was supported by inspection of contours of these values on maps of potential vorticity.

Then, for each of the starting θ surfaces, the parcels' ending θ values were subtracted to get the average descent over this period. Figure 4 shows the result. Parcels starting at 600 K

Figure 4

in mid-January had descended by some 40 K, on average, by mid-March. Parcels in the lower stratosphere, between 400 and 500 K, descended roughly 15 to 20 K during the same time. To get the average diabatic descent as a function of initial potential temperature, two straight lines were fit to the data, meeting at 475 K.

To determine ozone loss, ozone fields were reconstructed on January 10 and March 17 on a series of pairs of potential temperature surfaces within the vortex, the March 17 surface being adjusted upward to compensate for the descent of air within the vortex. The ozone decline was calculated by differencing these two vertical profiles; this method will be referred to as the "vortex average descent" method below.

The second method used to remove diabatic effects to determine ozone loss involved tracing the parcel trajectories of the ozone measurements themselves. If the trajectory model were perfect, then parcels started on January 10 with certain PV and θ coordinates would end on March 18 with different values of PV and θ. If these "diabatically adjusted" PV-θ coordinates are used in the linear time fits, then the slopes of those fits should reflect chemical loss alone. This method will be termed the "diabatic coordinate adjustment" technique in the discussion which follows.

Of course, trajectories of individual parcels cannot be traced accurately for such long periods, but TRAJREF indicates that reasonable results can be obtained using large ensembles of trajectories whose results are averaged together.

4. Results

4.1. Vortex Average Descent Method

To apply the vortex average descent method of determining loss, ozone measurements from the ER-2 in situ instrument, the DC-8 AROTEL and DIAL lidar instruments, and the THESEO ozonesondes were combined into a single PV-θ composite. Random points from each instrument were discarded until their measurements were of approximately equal density in PV-θ space, so that no one instrument would dominate the analysis. The resulting composite was used to reconstruct ozone on potential temperature surfaces for January 10 and March 17. The surfaces for March 17 were adjusted upwards to account for diabatic descent as determined by the fit in Figure 4. Reconstructed gridpoints of ozone in the core of the vortex were selected and area-averaged to obtain two vertical profiles, one at each end of the time period being examined.

Figure 5 shows these profiles. The difference between these curves, divided by the time period, is the average chemical ozone loss rate. The ozone loss rate calculated here peaks at 470 K with a value of 0.026 ppmv/day and decreased to near 0 at 650 to 700 K. Results are shown using the NCAR/NCEP Reanalysis; the UKMO analyses and DAO data produce similar curves with loss rates of 0.025 and 0.026, respectively, at 470 K.

Figure 5

The profiles in Figure 5 extend down to 350 K and show the loss rates continuing to shrink below the 400 K level. Although the PV-θ technique is more suitable for use in the stratosphere, where (modified) PV and θ are at least quasi-conserved and quasi-orthogonal, the technique seeems to yield reasonable values down into the very lowest part of the stratosphere

and into the uppermost troposphere.

4.2. Diabatic Coordiate Adjustment Method

To apply the diabatic coordinate adjustment technique, measurements from the THESEO sondes were used, since they were sparse enough that their trajectories could be traced easily. All days' sonde profiles were run forward to March 18 to obtain their diabatically adjusted PV and θ values on that date. They were also run backward to obtain their diabatically adjusted PV and θ values on January 10. Parcels whose PV changed by more than 25% over this period were discarded to reduce the effects of parcels entering or leaving the vortex. The remaining measurements, with their adjusted PV-θ coordinates, were then used to construct a time-varying composite, and the slopes from the resulting time fits were obtained. Uncertainties in the slopes were also computed from the covariance matrices of the time fit coefficients (as in *Meyer* [1975]).

The loss rates were mapped onto vertical profiles in the vortex core; Figure 6 shows the area-weighted average of these profiles. Figure 6a shows the results for the forward trajectory run on January 10. The loss rate peaks at 0.032 ± 0.007 ppmv/day at 460 K. This is larger than that computed from the vortex averaged descent method, but it peaks in about the same altitude. (Vortex averaged descent loss rates computed from the ozonesonde data alone had the same peak location and value as from the composite of all the instruments.) Figure 6b shows the results for the back trajectory run on March 17; the loss rate peaks around 0.30 ± 0.008 ppmv/day at 440 K. The peak is about the same magnitude (indicating agreement between the forward and back trajectory runs), but it is located about 20 K lower in potential temperature

Figure 6

because of diabatic descent.

The back trajectory loss rates mapped to the January 10 profile are very similar to the forward trajectory rates for that date. Likewise, the forward trajectory results mapped to March 17 are similar to the back trajectory results for that date. That is, both trajectory runs show similar peak loss rates which descend in θ over the time period examined. Figure 7 shows both rates mapped onto February 13 profiles (the middle of the period). One difference between the two runs is that the forward trajectory profiles exhibit a small offset near the bottom of the profile (and are very nearly zero at the top), while the backward trajectory profiles show a small offset near the top of the profiles (and are very nearly zero at the bottom).

Figure 7

Figure 8 shows the time fit slopes (from the backwards trajectory run) for the 440 K surface as a function of equivalent latitude (*Butchart and Remsberg*, 1986) for February 13. The area-weighted average loss rate within the inner vortex region on the 440 K surface is 0.030 ± 0.009, as shown in the profile. Expanding the average to include most of the vortex decreases the loss rate slightly to 0.028 ± 0.007 at 440 K.

Figure 8

Results from the backwards trajectory run are similar within the vortex, but the change rates outside the vortex vary greatly between the two runs (from approximately -0.01 ppmv/dat to $+0.02$ ppmv/day at 470 K). The near-zero loss rate shown in Figure 8 outside the vortex must be considered largely fortuitous.

From Equation 1, the loss rate of total ozone O_T becomes:

$$\partial O_T/\partial t = \partial(W \int_0^{p_s} \chi dp)/\partial t \quad (3)$$

$$= W \int_0^{p_s} b(PV, \theta) dp + W \chi(p_s) \partial p_s/\partial t \quad (4)$$

where $W = 0.789\ \mathrm{m\ s^2/kg}$ and p_s is the surface pressure. We do not reconstruct ozone values in the lower troposphere, but fixing the (notional) ozone profile to zero at the surface (as is done to derive the total ozone values mapped in Figure 3) makes the second term vanish. (As a dynamical effect, the second term has no bearing on chemical ozone loss anyway.) Thus, integrating the time slopes yields that part of the time rate of change of total ozone which is caused by chemical destruction.

Time fit slopes from the diabatically-adjusted sonde data were mapped onto vertical profiles as a function of pressure. Loss rates from the back trajectory results were used because they were close to zero below 400 K, a region more heavily weighted in the integration. Any ozone increases (i.e., from the offsets near the top of the profiles) were zeroed out—only ozone destruction rates are of interest. These rate profiles were then integrated and area-averaged within the vortex core for each day between January 10 and March 17.

Figure 9 shows the daily total ozone loss rates for the core of the vortex. The losses begin at approximately 0.8 DU/day and increase to 1.3 DU/day by March 17. The loss rates' evolution is associated with both a descent in the peak altitude of ozone loss and a shift in the PV values associated with the vortex core, with the latter dominating. Summing the daily loss rates yields a decrease of about 77 DU caused by chemical loss of ozone.

Figure 9

5. Discussion and Conclusions

Ozone measurements from AROTEL, DIAL, the NOAA ER-2 instrument, and the THESEO ozonesondes have been combined using a PV-θ analysis technique which allows the ozone field to evolve in time. Realistic ozone fields have been obtained by mapping the

ozone field from PV-θ coordinates back into real space. Diabatic effects have been estimated using modeled trajectories of large numbers of parcels. Estimates of chemical ozone loss in the lower stratosphere are found peak at 0.030 ± 0.009 ppmv/day near 460 K in January, with this peak descending to 440 K in March. The loss near 450 K is thus about 2 ppmv over the period. The loss rates also decrease to near 0 at 550 to 600 K.

The PV-θ analysis has several potential pitfalls. It depends on its constituent being long-lived enough to be well-mixed along contours of isentropic potential vorticity. In the middle stratosphere and above, where photochemistry dominates, the method is of limited applicability to ozone. This analysis has been confined to the lower stratosphere.

When an ozone measurement is made near the vortex edge in the sunlight, where chlorine-driven photochemical destruction is likely to be enhanced, this measurement may not be typical of ozone values around a PV contour on a θ surface that intersects the measurement location. With enough additional measurements around that contour, PV-θ analysis will yield an averaged view of the ozone field which the ozone-depleted measurements will influence but not necessarily dominate. Poor sampling, however, may lead to the sunlit region being under-represented or over-represented in the average until the ozone-depleted air is mixed along the contour. This analysis relies on the time series fit to average out the sudden drops in ozone that might appear in such cases.

To distinguish between diabatic effects and chemical destruction of ozone, this analysis uses diabatic trajectories of large numbers of parcels traced over about ten weeks. Averaging the effects of large numbers of parcels might well compensate for the inaccuracy of individual parcel trajectories, but there remains the possibility of systematic artifacts of the

meteorological analysis used or of the radiation model used to generate the heating rates.

The diabatic heating rates have been verified in previous work (*Rosenfield et al.* [submitted]) for the UKMO meteorological products, and they appear to be reasonable.

Another approach would be to analyze a tracer such as N_2O and test whether the diabatic trajectories reduce the apparent rate of change, which should be a purely diabatic effect. This has been attempted, and the results suggest that using diabatically-adjusted trajectories tends to reduce the rates of change in the vortex core at altitudes higher than 500 K. However, the N_2O measurements from SOLVE were sparse enough, and the uncertainties in the rates are consequently large enough to make these results inconclusive. That is, the differences between the uncorrected rate profiles and the diabatically corrected rate profiles are smaller than the uncertainties in either.

Another effect which would complicate matters is mixing across the vortex boundary. Although the polar vortex is generally recognized as being isolated from the midlatitudes (*Bowman* [1993], *Schoeberl et al. [submitted]*), it is not completely isolated—slow or weak mixing may occur over the course of a season, in addition to occasional major intrusion events such as one described by *Plumb et al.* [1994]. The PV-θ technique may still reconstruct ozone fields with some degree of fidelity in these circumstances, but untangling chemical destruction from mixing becomes problematic. In this analysis, the issue is addressed by excluding parcels whose diabatic trajectories involved a change of PV of more than 25%, but it is unclear whether this is sufficient given the limitations of tracing individual parcels. In other words, it is difficult to say whether a parcel has been excluded because it moved into or out of the vortex, or because its trajectory is simply not accurately traced.

Inspection of the gridpoint trajectories used to determine descent rates shows only a few cases where trajectories which originated outside the vortex in January ended up inside the vortex in March: about 1.3% of the mid-March vortex parcels at 420–430 K for the back-trajectories only. For other theta levels and for the forward trajectory run, no such parcels were found. *Schoeberl et al.* [in press], which used a more comprehensive trajectory modelling run, supports the assertion that mixing into the vortex was negligible over most of this period.

Toward the middle of March, as the vortex was breaking up, the effects of mixing are expected to increase. A sharper drop-off in ozone at the end of the time series can be seen in Figure 1, and it is difficult to say how much of this is caused by mixing and how much by chemical destruction in the increased sunlight. This analysis partially side-steps the issue by fitting a linear trend over the 10-week period, so that the sudden drop-off at the end does not influence the overall trend too strongly.

Other techniques have been used to categorize ozone loss. Instead of placing all the data into a composite time-dependent field, the MATCH program (*Rex et al.*, 1999) uses paired individual ozonesonde profiles to determine ozone loss. MATCH selects the pairs by tracing the trajectories of sonde-sampled air parcels until they intersect other sonde launches days later. By using small clusters of trajectories for each measurement, and by averaging differenced pairs together, MATCH tends to reduce the uncertainties associated with the trajectory calculations. Because MATCH uses changes in PV as a criterion in matching pairs of sonde launches, its ozone values are effectively categorized by PV in a way similar to PV-θ analysis. Instead of dealing with pairwise differences at discrete θ levels, though, the PV-θ

technique has the effect of averaging all ozone measurments of similar PV and θ values. More data will tend to enter such an average at the cost of a higher dependence upon the assumption than ozone is well-mixed along an isentropic PV contour.

The vortex-averaged analysis of Schoeberl et al. [submitted] involves diabatic trajectory calculations initialized from massive numbers of ozone measurement locations, so that the inaccuracies associated with individual parcels are averaged out. The data which remain inside the vortex are fit to a quadratic curve at various theta levels to obtain ozone loss rates from December 1999 through mid-March 2000. Solar exposure is also used to discriminate between parcels in the core of the vortex and parcels from the edge region.

The PV-θ technique with diabatic corrections may be thought of as a way of enhancing such a trajectory analysis to produce a continuously evolving ozone field. The peak ozone loss rates produced here are lower than MATCH's of 0.05 ppmv/day, but somewhat higher than the 0.025 ppmv/day obtained by the Schoeberl trajectory analysis. The peak loss rates seem to be a little lower and broader in altitude in the latter results, as well, but this may be an artifact of the heavy smoothing done here.

Acknowledgments. The author wishes to acknowledge the DC-8 and ER-2 pilots and the flight and ground crews who made the aircraft measurements possible under sometimes difficult conditions; the sonde launch personnel, who sent the balloons up under some very difficult conditions; the SOLVE logistics staff and the personnel of the Arena Arctica in Kiruna, Sweden, who made the conditions much less difficult there; and SOLVE and THESEO management. This research was supported by the NASA's Atmospheric Chemistry Modeling and Analysis Program and the Upper Atmosphere Research Program.

References

Bowman, K. P., Large scale isentropic mixing properties of the Antarctic polar vortex from analyzed winds, *J. Geophys. Res., 98*, 23013-23027, 1993.

Browell, E. V., S. Ismail, and W. B. Grant, Differential absorption lidar (DIAL) measurements from air and space, *Appl. Phys. B 67*, 399–410, 1998.

Butchart, N., and E. E. Remsberg, The area of the stratospheric polar vortex as a diagnostic for tracer transport on an isentropic surface. *J. Atmos. Sci., 43*, 1319–1339, 1986.

Farman, J. C., B. G. Gardiner, and J. D. Shanklin, Large losses of total ozone in Antarctica reveal seasonal ClO_X/NO_X interaction, *Nature, 315*, 207–210, 1985.

Kalnay, E., M. Kanamitsu, R. Kistler, W. Collins, D. Deaven, L. Gandin, M. Iredell, S. Saha, G. White, J. Woollen, Y. Zhu, M. Chelliah, W. Ebisuzaki, W. Higgins, J. Janowiak, K. C. Mo, C. Ropelewski, J. Wang, A. Leetmaa, R. Reynolds, R. Jenne, and D. Joseph, The NCEP/NCAR 40-year reanalysis project, *Bull. Am. Met. Soc., 77*, 437–471, 1996.

Kyrö, E., R. Kivi, T. Turunen, H. Aulamo, V. V. Rudakov, V. Khattatov, A. R. MacKenzie, M. P. Chipperfield, A. M. Lee, L. Stefanutti, and F. Ravegnani, Ozone measurements during the Airborne Polar Experiment: aircraft instrument validation, isentropic trends, and hemispheric fields prior to the 1997 Arctic ozone depletion, *J. Geophys. Res., 105*, 14599–14611, 2000.

Lait, L., An alternative form for potential vorticity, *J. Atmos. Sci., 51*, 1754–1759, 1994.

Lait, L. R., M. R. Schoeberl, P. A. Newman, M. H. Proffitt, M. Lowenstein, J. R. Podolske, S. E. Strahan, K. R. Chan, B. Gary, J. J. Margitan, E. Browell, M. P. McCormick, and A. Torres, Reconstruction of O3 and N2O fields from ER-2, DC-8, and balloon observations, *Geophys. Res. Lett., 17*, 521–524, 1990.

Leovy C. B., C. R. Sun, M. H. Hitchmann, E. E. Remsberg, J. M. Russel III, L. L. Gordley, J. C. Gille, and L. V. Lyjack, Transport of ozone in the middle stratosphere: evidence for wave breaking. *J. Atmos. Sci., 42*, 230–244, 1985.

Manney G. L., L. Froidevaux, M. L. Santee, R. W. Zurek, J. W. Waters, MLS observations of Arctic ozone loss in 1996-97, *Geophys. Res. Lett., 24*, 2697–2700, 1997.

McGee, T. J., J. Burris, et al., AROTEL: an airborne ozone, aerosol, and temperature lidar, *this issue of J. Geophys. Res.*, 2001.

Morris, G. A., J. F. Gleason, J. Ziemke, M. R. Schoeberl, Trajectory mapping: a tool for validation of trace gas observations, *J. Geophys. Res., 105*, 17875–17894, 2000.

Meyer, Stewart L., *Data Analysis for Scientists and Engineers*, 513 pp., John Wiley, New York, 1975.

Newman P. A., J. F. Gleason, R. D. McPeters, R. S. Stolarski, Anomalously low ozone over the Arctic, *Geophys. Res. Lett., 24*, 2689–2692, 1997.

Pfaendtner, J., S. Bloom, D. Lamich, M. Seablom, M. Sienkiewicz, J. Stobie, and A. da Silva, Documentation of the Goddard Earth Observing System (GEOS) Data Assimilation System - Version 1, NASA Technical Memorandum 104606, Vol. 4, 1995.

Plumb, R. A., D. W. Waugh, R. J. Atkinson, P. A. Newman, L. R. Lait, M. R. Schoeberl, E. V. Browell, A. J. Simmons, and M. Lowenstein, Intrusions into the lower stratosphere Arctic vortex during the winter of 1991–1992, *J. Geophys. Res., 99*, 1089–1105, 1994.

Proffitt, M. H., and R. J. McLaughlin, Fast-response dual-beam UV absorption ozone photometer suitable for use on stratospheric balloons, *Rev. Sci. Instrum., 54*, 1719–1728, 1983.

Rex, M., P. von der Gathen, G. O. Braathen, S. J. Reid, N. R. P. Harris, M. Chipperfield, E. Reimer, A. Beck, R. Alfier, R. Kruger-Carstensen, H. De Backer, D. Balis, C. Zerefos, F. O'Conner,

H. Dier, V. Dorokhov, H. Fast, A. Gamma, M. Gil, E. Kyrö, M. Rummukainen, Z. Litynska, I. S. Mikkelsen, M. Molyneux, and G. Murphy, Chemical ozone loss in the Arctic winter 1994/1995 as determined by the Match technique, *J. Atmos. Chem., 32*, 35–39, 1999.

Rodriguez, J., Probing stratospheric ozone, *Science, 261*, 1128–1129, 1993.

Rosenfield, J. E., P. A. Newman, and M. R. Schoeberl, Computations of diabatic descent in the stratospheric polar vortex, *J. Geophys. Res., 99*, 16677–16689, 1994.

Rosenfield, J. E., and M. R. Schoeberl, On the origin of polar vortex air, *J. Geophys. Res., submitted.*

Salawitch, R. J., S. C. Wofsy, E. W. Gottlieb, L. R. Lait, P. A. Newman, M. R. Schoeberl, M. Lowenstein, J. R. Podolske, S. E. Strahan, M. H. Proffitt, C. R. Webster, R. D. May, D. W. Fahey, D. Baumgardner, J. E. Dye, J. C. Wilson, K. K. Kelly, J. W. Elkins, K. R. Chan, J. G. Anderson, Chemical loss of ozone in the Arctic polar vortex in the winter of 1991-1992, *Science, 261*, 1146–1149, 1993.

Schoeberl M. R. and L. R. Lait, Conservative coordinate transformations for atmospheric measurements, in *Proc. Internat. School of Phys. "Enrico Fermi", CXV Course*, edited by J. C. Gille and G. Visconti, 419-430, 1991.

Schoeberl, M. R., P. A. Newman, L. R. Lait, T. J. McGee, J. F. Burris, E. V. Browell, W. B. Grant, E. C. Richard, P. von der Gathen, R. Bevilacqua, I. S. Mikkelsen, M. J. Molyneux, An Assessment of the Ozone Loss During the 1999-2000 SOLVE/ THESEO 2000 Arctic Campaign, *J. Geophys. Res., submitted.*

Schoeberl, M .R., C. H. Jackman, and J. E. Rosenfield, A Lagrangian estimate of aircraft effluent lifetime, *J. Geophys. Res., 103*, 10817–10825, 1998.

Schoeberl, M .R., L. R. Lait, P. A. Newman, R. L. Martin, M. H. Proffitt, D. L. Hartmann,

M. Lowenstein, J. Podolske, S. E. Strahan, J. Anderson, K. R. Chan, and B. Gary, Reconstruction of the constituent distribution and trends in the Antarctic polar vortex from ER-2 flight observations, *J. Geophys. Res., 94,* 16815–16845, 1989.

Swinbank, R., and A. O'Neil, A stratosphere-troposphere data assimilation system, *Mon. Wea. Rev., 122*, 686–702, 1994.

Turco R., A. Plumb, E. Condon, The airborne arctic stratospheric expedition–prologue, *Geophys. Res. Lett., 14*, 313–316, 1990.

L. Lait, Code 916, NASA Goddard Space Flight Center, Greenbelt, MD 20071

Received May 31, 2001

Submitted for publication in *JGR*, 2001.

Figure 1. Time series of ozonesonde mixing ratio measurements near PV=32 PVU and θ=450 K. The gray shading of each symbol indicates its weighting in the linear time fit; the size of each symbol indicates its proximity to the PV-θ gridpoint. The linear time fit and its uncertainty ($\pm$ one standard deviation) are overlaid. Dashed vertical lines mark February 1 and March 1.

Figure 2. Ozone as a function of flight time and altitude for the DC-8 flight of 2001-03-09, (a) as measured by the AROTEL instrument on board the DC-8, (b) using THESEO ozonesonde measurements mapped into PV-θ space and then mapped onto the AROTEL measurement locations.

Figure 3. (a) Total ozone fields as measured by TOMS (left) and as calculated from sonde, lidar, and ER-2 ozone data using the PV-θ reocnstruction technique (right). (b) Scatter plot of reconstructed values versus the TOMS measurements.

Figure 4. Vortex descent between 2000-01-10 and 2000-03-18 as a function of starting potential temperature. Crosses mark parcels from forward trajectories, and diamonds mark parcels from backward trajectories. Two linear least-squares fits have been drawn through the points.

Figure 5. (a) Reconstructed ozone profiles (area-averaged over the core of the vortex) from January 12 (right line) and March 17 (left line). The March profile has had its θ values adjusted to remove diabatic descent over the period. (b) Ozone loss rates for the vortex core, calculated by subtracting the two curves from (a).

Figure 6. Ozone loss rate (from the time fit slopes of diabatically-adjusted sonde data) as a function of θ for the vortex core region for (a) January 10 using diabatic corrections from forward trajectories and (b) March 17 using diabatic corrections from back trajectories.

Figure 7. Same as Figure 6, except both ozone loss rates have been mapped for February 13 for both forward and back trajectory results.

Figure 8. Ozone loss rate (from the time fit slopes of diabatically-adjusted sonde data) as a function of equilalent latitude at the 440 K θ surface on February 13, 2000. The vertical dotted line marks the core of the polar vortex.

Figure 9. Vertically integrated chemical ozone loss rates for January 10 through March 17, within the core of the polar vortex.

Ozonesondes Ozone (ppmv)
2000-01-10T00 to 2000-03-18T00
MPV= 32.0000 PVU, Theta= 450.000 K
Met data = UARS UKMO

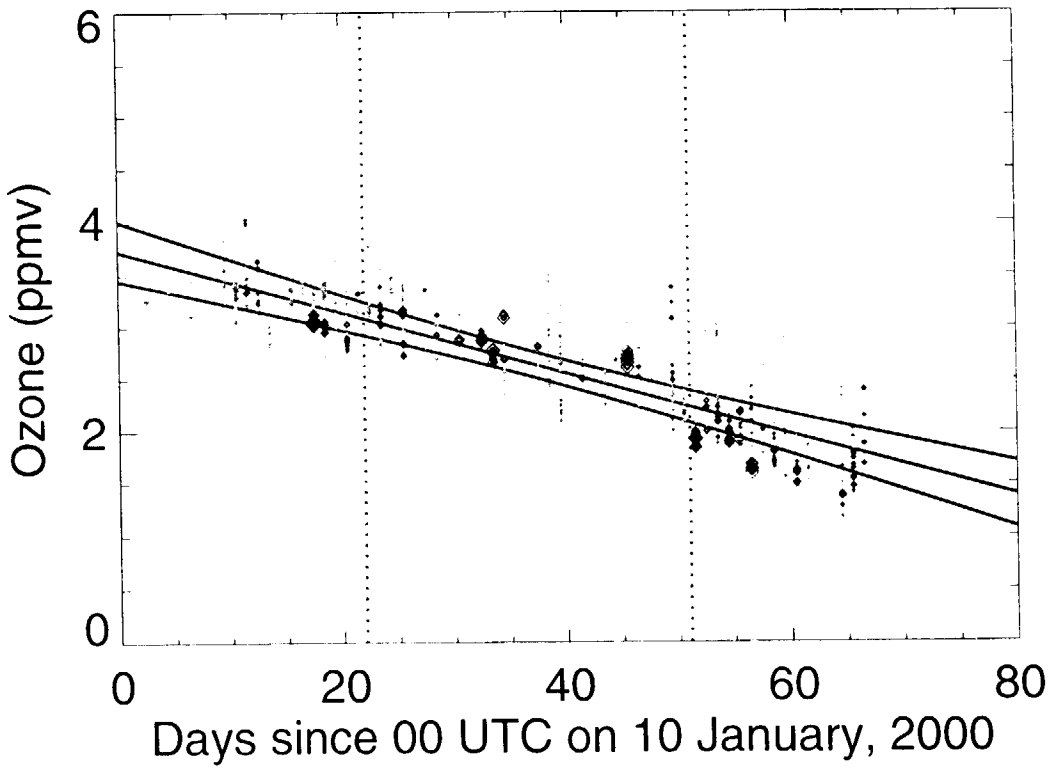

Slope = -0.0292 +/- 0.00678 ppmv/day

Figure 1

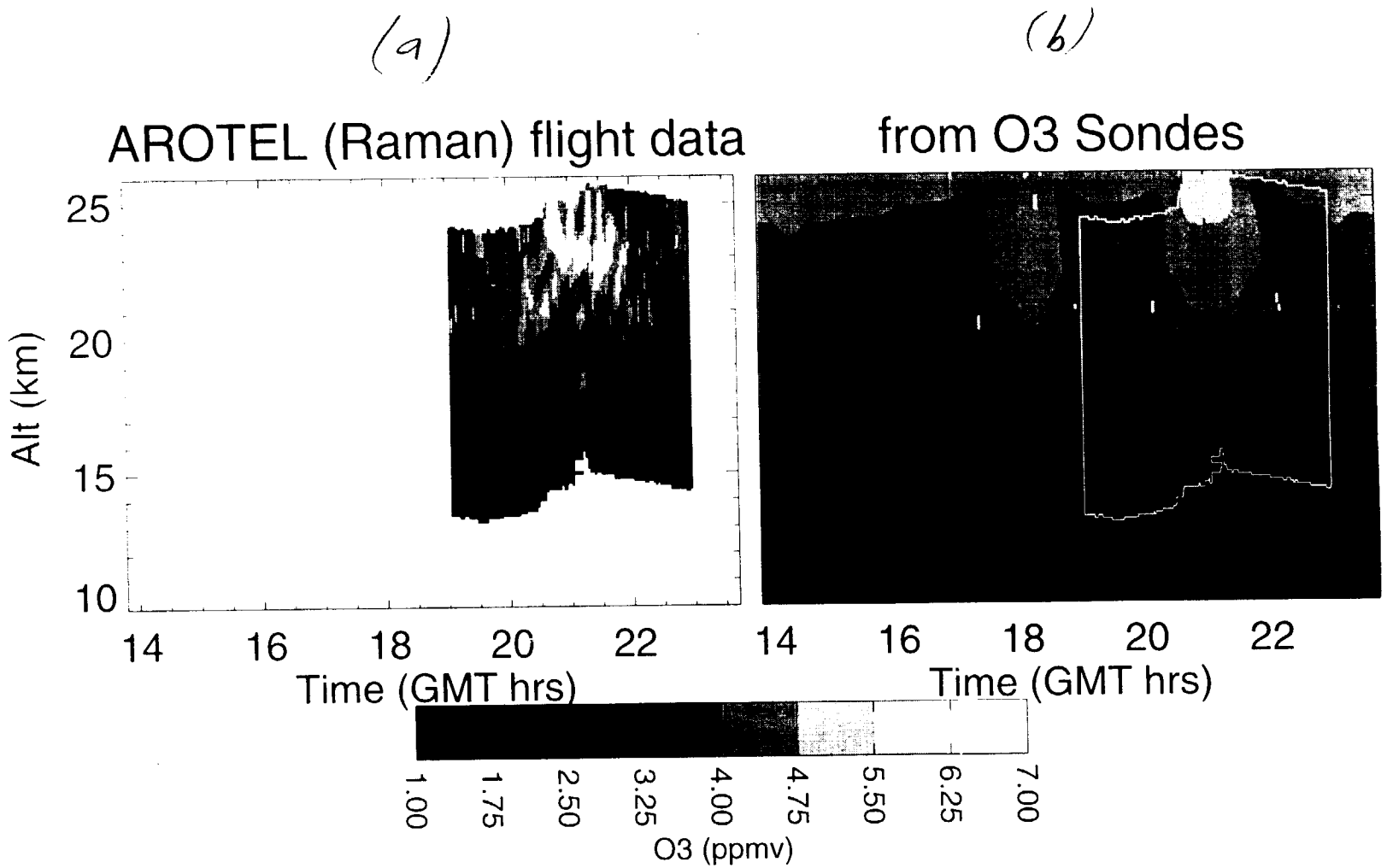
DC-8 flight of 9 March, 2000
(Using DAO 1X1 FLK)
(a)
(b)
AROTEL (Raman) flight data
from O3 Sondes
Alt (km)
25
20
15
10
14
16
18
20
22
Time (GMT hrs)
Time (GMT hrs)
1.00
1.75
2.50
3.25
4.00
4.75
5.50
6.25
7.00
O3 (ppmv)

Figure 2

Reconst. Total Ozone from All Sources
10 March, 2000

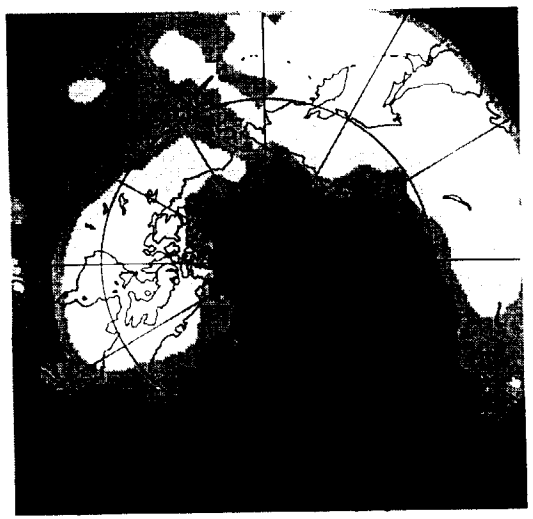

TOMS Tot. O3

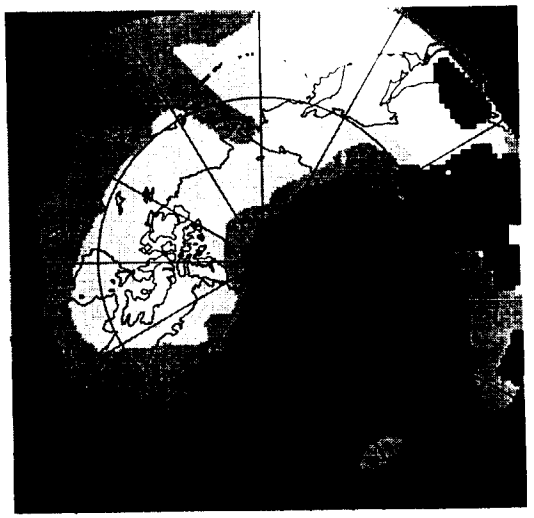

Rec. Tot. O3

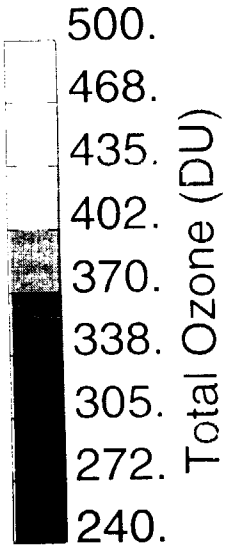

Figura 3a

Reconst. Total Ozone from All Sources
10 March, 2000

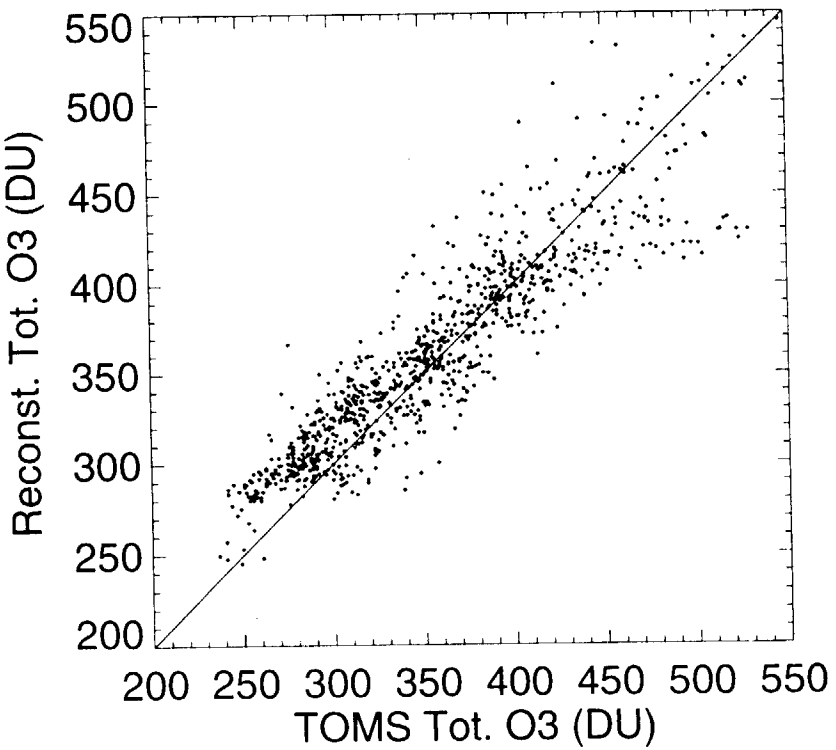

Frame 36

Diabatic Descent: 2000-01-10 to 2000-03-18

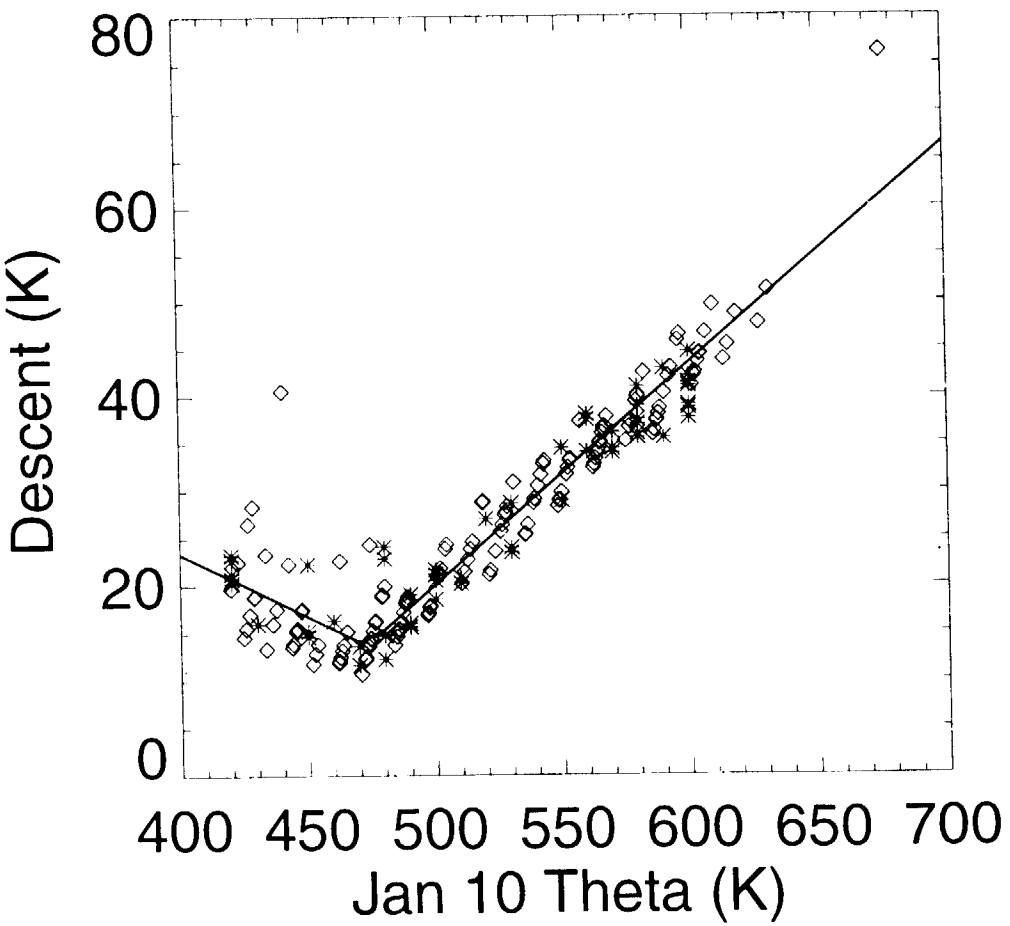

Figure 4

AROTEL+DIAL+Sondes+ER-2 Ozone Reconst.
12 UTC on 10 January, 2000 to 12 UTC on 17 March, 2000

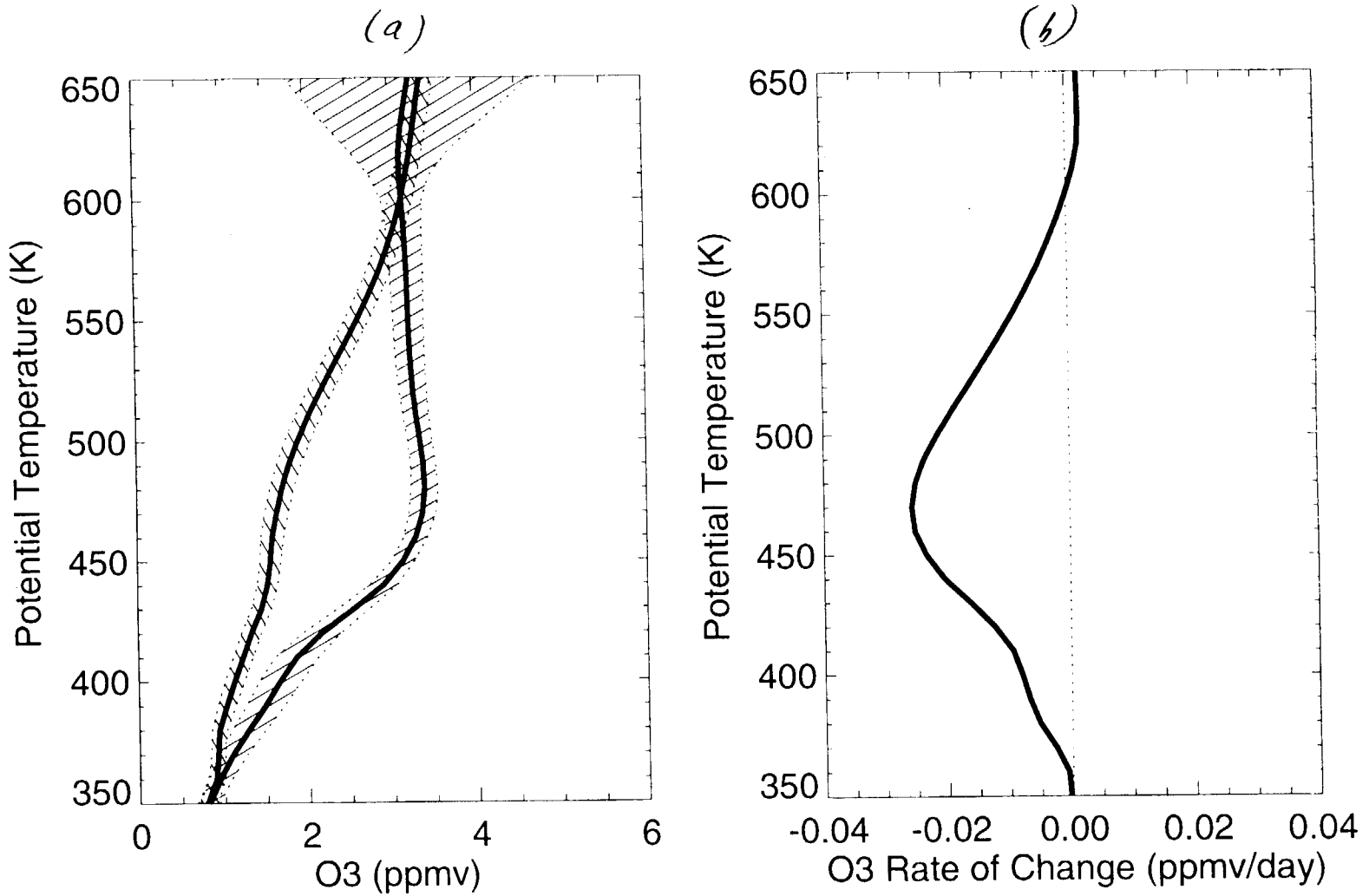

(Using NCEP Reanlysis met data)

(Constant diabatic correction)

2000-01-10T00%2000-03-18T00__GMHAM_E01_PTHINFIT_SCOMBO_MREAN

Figure 5

Diabatically Adjusted O3 Sondes (Fwd, Filt)
12 UTC on 10 January, 2000

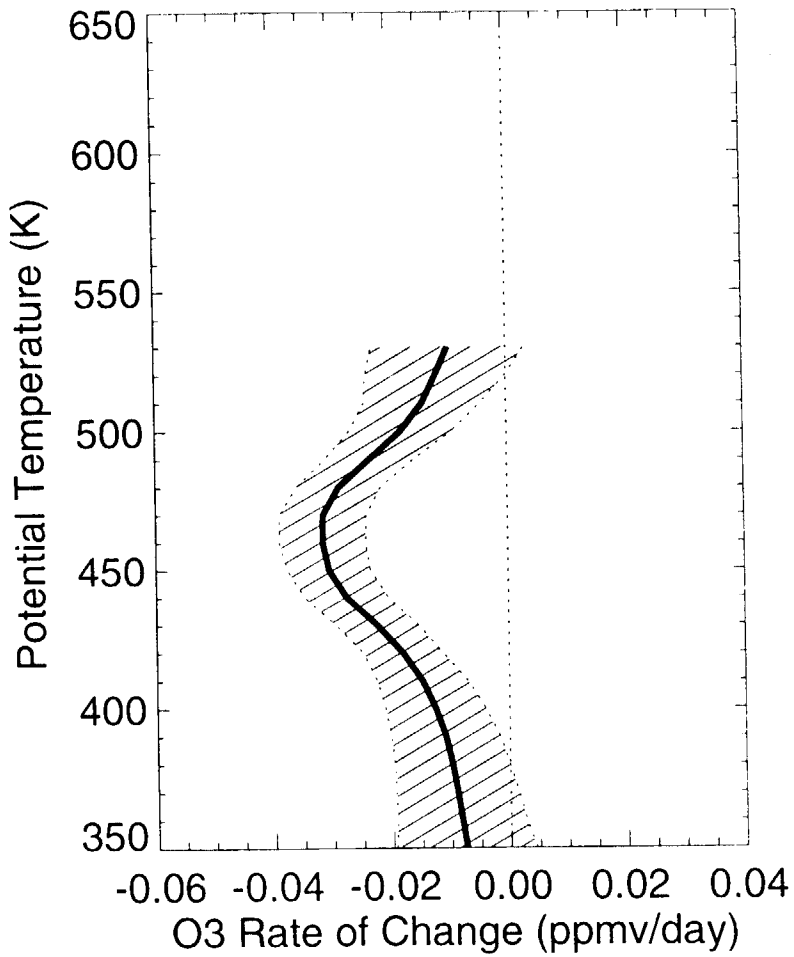

(Using UARS UKMO met data)

2000-01-10T00%2000-03-18T00__GMHAM_E01_PTHINFIT_SXFSONDES_MUKM

Fig 6a

Diabatically Adjusted O3 Sondes (Bck, Filt)
12 UTC on 17 March, 2000

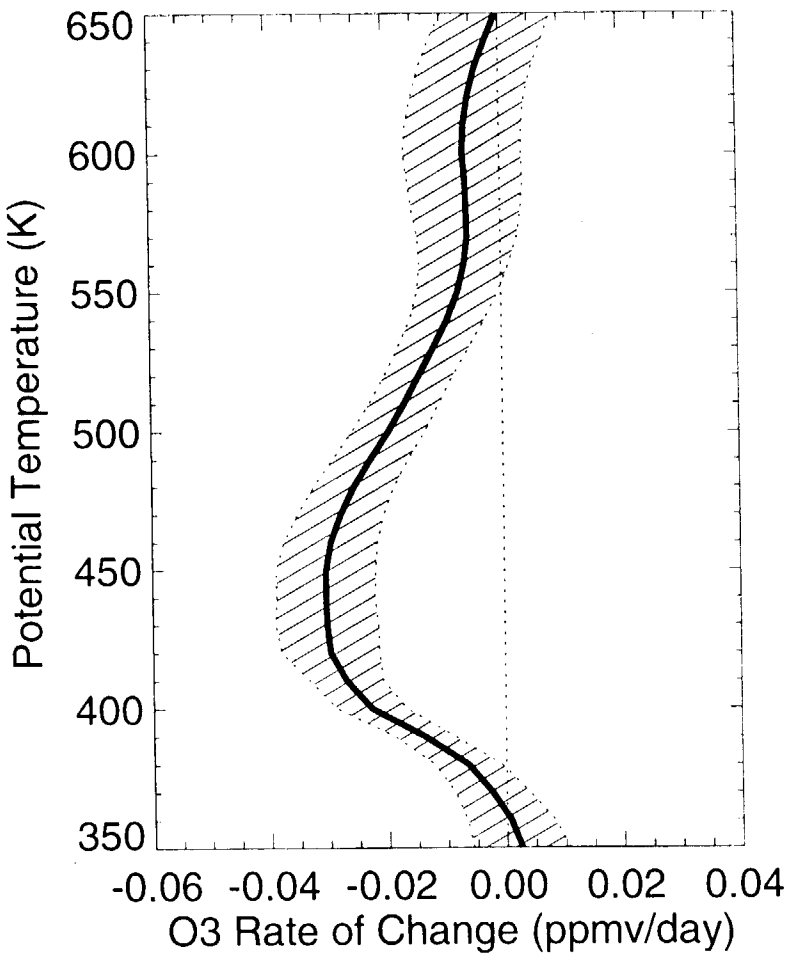

(Using UARS UKMO met data)

2000-01-10T00%2000-03-18T00__GMHAM_E01_PTHINFIT_SXBSONDES_MUKM

Fig. 66

Diabatically Adjusted O3 Sondes (Fwd, Filt)
12 UTC on 13 February, 2000

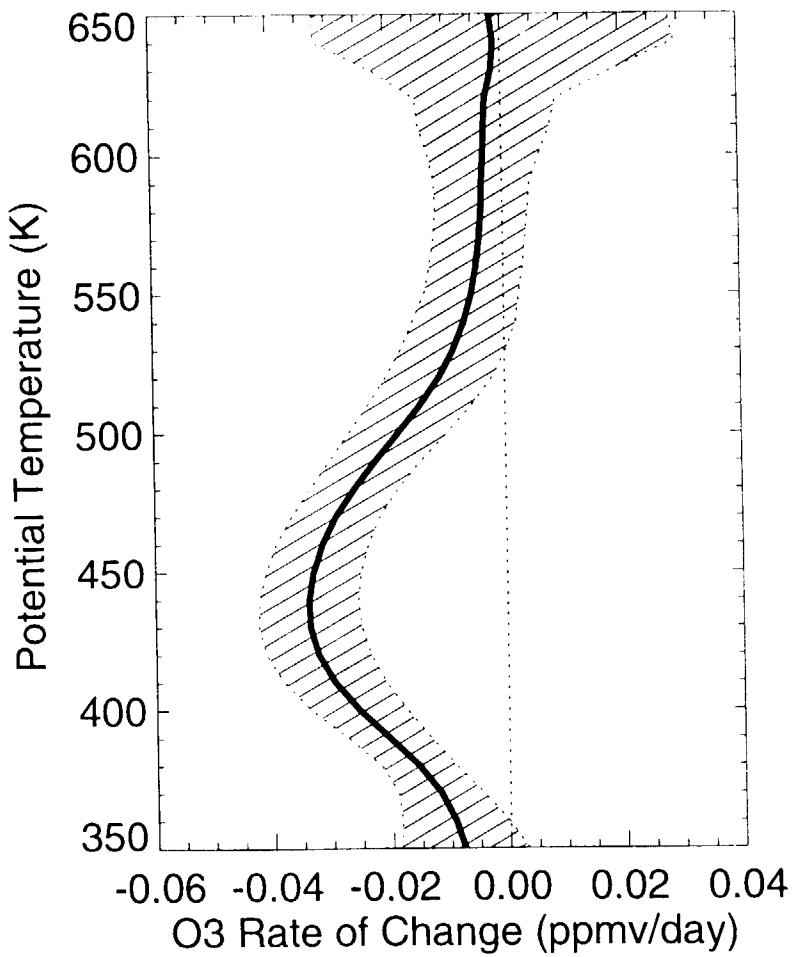

(Using UARS UKMO met data)

2000-01-10T00%2000-03-18T00__GMHAM_E01_PTHINFIT_SXFSONDES_MUKM

Fig 7a

Diabatically Adjusted O3 Sondes (Bck, Filt)
12 UTC on 13 February, 2000

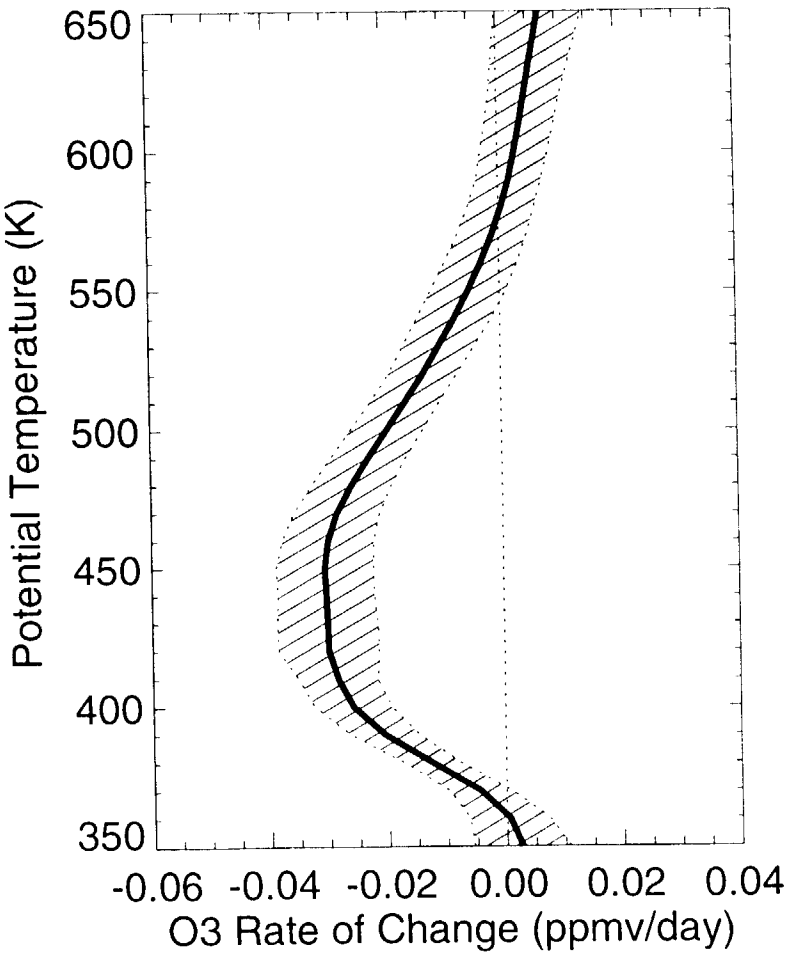

(Using UARS UKMO met data)

2000-01-10T00%2000-03-18T00__GMHAM_E01_PTHINFIT_SXBSONDES_MUKM

Fig 76

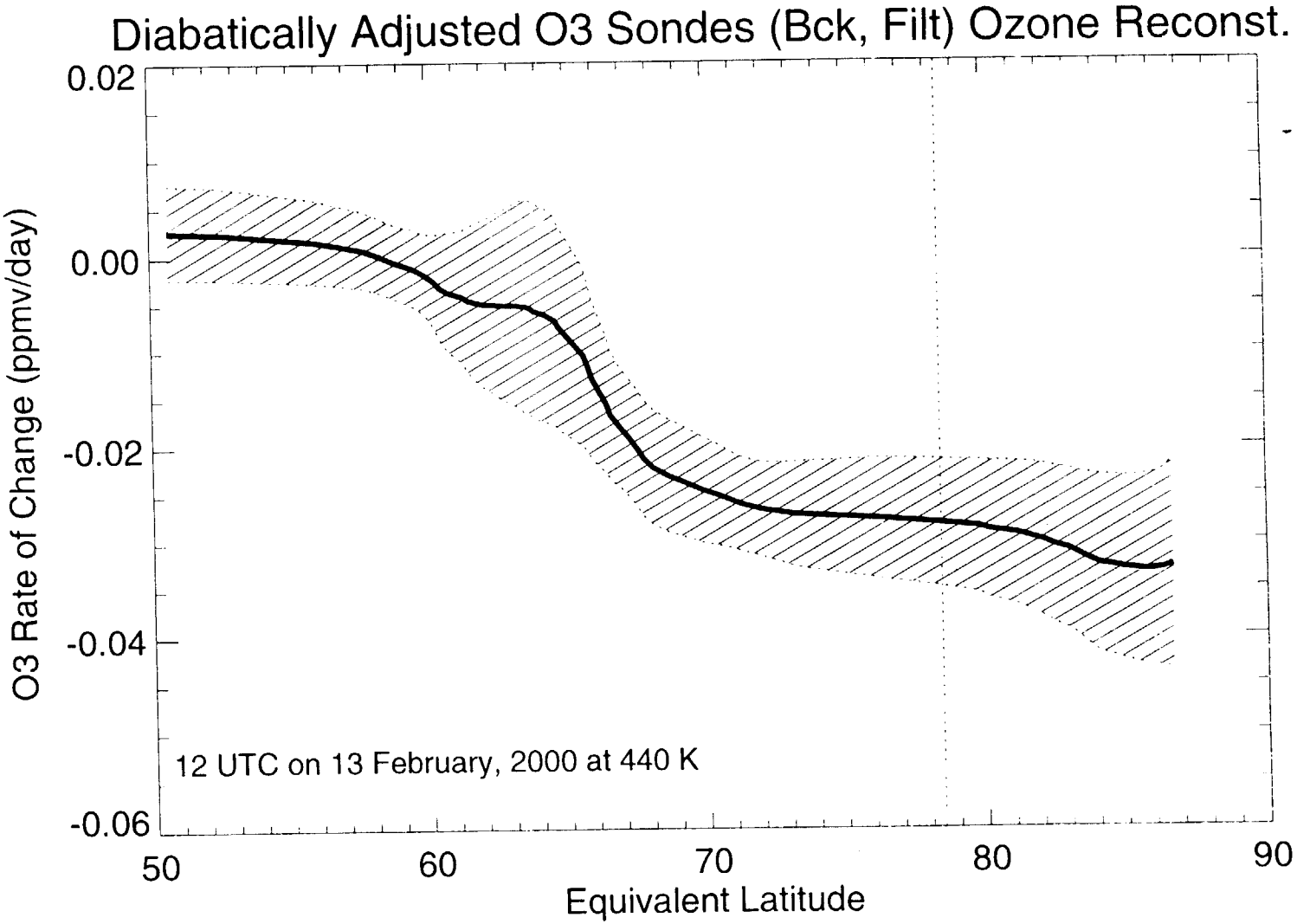

(Using UARS UKMO met data)

2000-01-10T00%2000-03-18T00__GMHAM_E01_PTHINFIT_SXBSONDES_MUKM

Fig 8

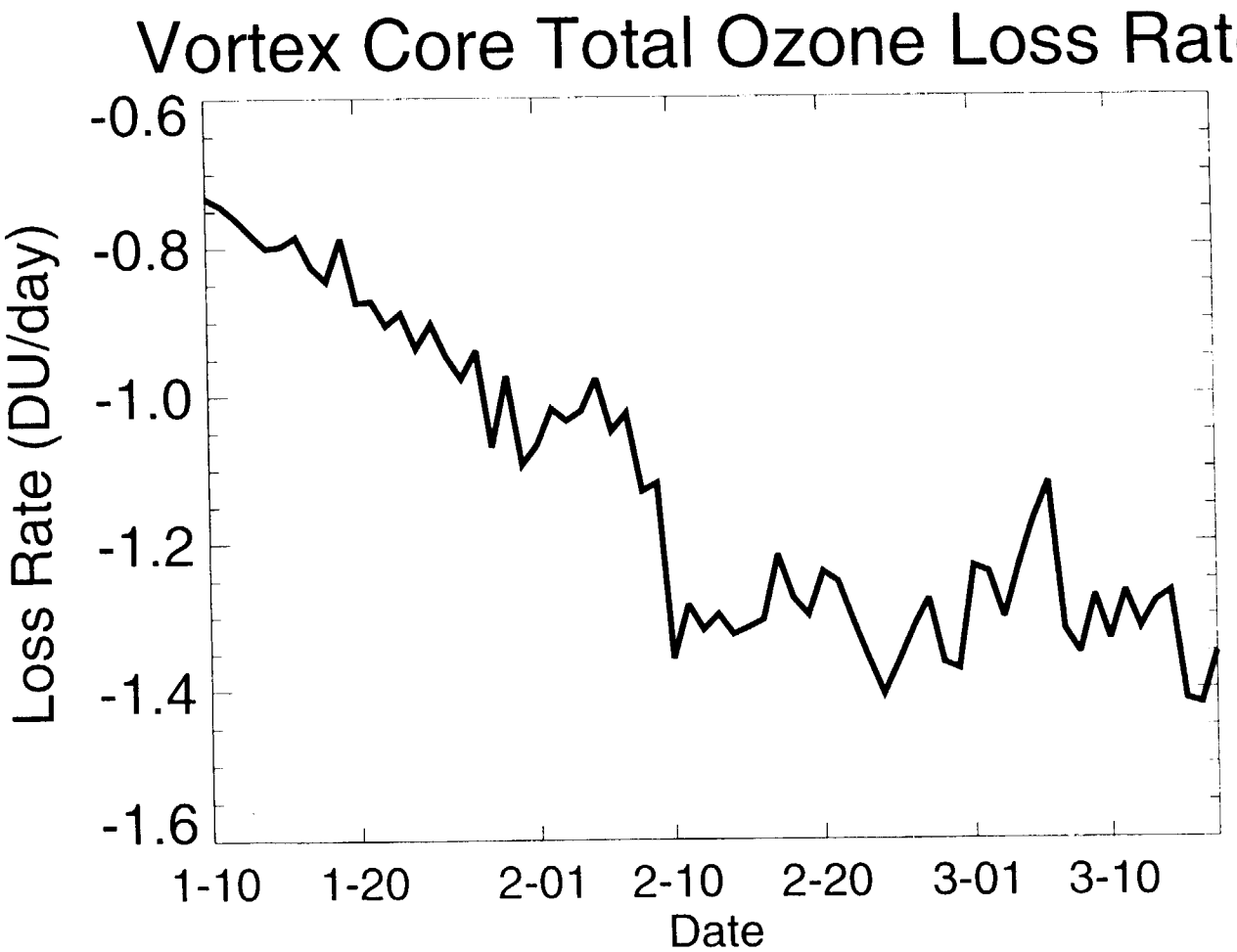

Diabatically Adjusted O3 Sondes (Bck, Filt)
(UARS UKMO met data)

Fig 9